Theoret. Chim. Acta (Berl.) 47, 85–96 (1978)

THEORETICA CHIMICA ACTA

Original Investigations

Numerical Integration of Overlap and Ligand Contributions to the Electric Field Gradient*

Reiner Reschke and Alfred Trautwein

Fachbereich Angewandte Physik, Universität des Saarlandes, D-6600 Saarbrücken, Federal Republic of Germany

The total electric field gradient (EFG) tensor V_{pq} is calculated by numerical integration of threedimensional integrals. Each of them is solved a) by integrating over one dimension analytically and b) by integrating over the remaining two dimensions on the basis of a Gauss-type integration rule. The use of 100 abscissas in the twodimensional numerical integration scheme yields satisfactory accuracy which was checked by evaluating overlap integrals; an increase to 400 abscissas does not increase the result drastically. Calculating quadrupole splittings ΔE_Q from numerically integrated electric field gradient tensors V_{pq} we observe that depending a) on the amount of covalency and b) on the amount of deviation from octahedral or tetrahedral symmetry, involved in a molecular system, overlap and ligand contributions to V_{pq} play an important role. Especially for the sandwich compound ferrocene, $Fe(C_5H_5)_2$, we find a significant difference between $\Delta E_Q^{\text{num. int.}}$ which follows from the numerical integration method, and $\Delta E_Q^{\text{conventional}}$ which is derived from effective charges.

Key words: Electric field gradient, total, calculation of ~

1. Introduction

In molecular systems with high covalency it is sometimes a too crude approximation to calculate the electric field gradient (EFG) tensor at the nuclear site of atom A from valence electrons of A and from effective charges at ligand sites B only [1–3]; this approximation implies that all charges within the molecular system under study – besides the valence electrons of A – are lumped together to effective point charges at B while the space between A and B, and between sites B is "empty".

* Supported by Deutsche Forschungsgemeinschaft

0040-5744/78/0047/0085/$02.40

A more rigorous treatment of the problem is to divide the total charge of the molecular system into positive point charges (nuclear charge plus charge of core electrons) located at atomic sites, and into a charge distribution of valence electrons which may be derived from molecular orbital (MO) calculations.

2. General

Following the idea to calculate the EFG tensor V_{pq} (for example at the nuclear site of a Mössbauer atom A) from the positive point charges (located at ligand sites B) and from the whole valence electron charge distribution within the system under study, we have two contributions:

$$V_{pq} = V_{pq}^{\text{ligand cores}} + V_{pq}^{\text{valence electrons}}. \tag{1}$$

The first term in Eq. (1) is given by:

$$V_{pq}^{\text{ligand cores}} = \sum_{B \neq A} q_B [1 - \gamma(|\boldsymbol{r}_B - \boldsymbol{r}_A|)] \frac{3(r_p^B - r_p^A)(r_q^B - r_q^A) - \delta_{pq}|\boldsymbol{r}_B - \boldsymbol{r}_A|^2}{|\boldsymbol{r}_B - \boldsymbol{r}_A|^5}, \tag{2}$$

with $\boldsymbol{r}_A$ and $\boldsymbol{r}_B$ being space vectors locating atom A and B, respectively. The core charge of ligands B is q_B, and the quadrupole polarizability of the electronic shell of ion A is $\gamma(|\boldsymbol{r}_B - \boldsymbol{r}_A|)$ [1, 4]. The EFG contribution of all valence electrons is represented by the expectation value of the tensor operator

$$\hat{V}_{pq} = \sum_{i=1}^{N} [1 - \gamma(r_i)] \frac{3 r_p^i r_q^i - \delta_{pq} r_i^2}{r_i^5}, \tag{3}$$

where the summation is over all valence electrons, $i = 1, \ldots N$. The space vector $\boldsymbol{r}_i$ is given with respect to ion A. $V_{pq}^{\text{valence electrons}}$ then results from:

$$V_{pq}^{\text{valence electrons}} = -e_0 \langle \Psi | \hat{V}_{pq} | \Psi \rangle. \tag{4}$$

e_0 is the (positive!) elementary charge, and Ψ is the many-electron MO wavefunction, which describes the electronic configuration of the molecular system under study. In the Hartree-Fock approximation of MO calculations Ψ is a Slater determinant of orthonormal MO's, which are linear combinations of atomic orbitals (AO) ψ_μ [5, 6]. Eq. (4) can be rewritten in terms of atomic expectation values [7]:

$$V_{pq}^{\text{valence electrons}} = -e_0 \sum_{\mu\nu} P_{\mu\nu} \langle \psi_\mu | \hat{V}_{pq} | \psi_\nu \rangle. \tag{5}$$

Since the MO basis set consists of real AO's

$$\psi_\mu = f_\mu(r) Y_{l_\mu m_\mu}(\Omega), \tag{6a}$$

we are able to simplify the evaluation of atomic expectation values $\langle \psi_\mu | \hat{V}_{pq} | \psi_\nu \rangle$ by expressing the EFG tensor operator $\hat{V}_{pq}$ in terms of real spherical harmonics $Y_{lm}(\Omega)$

$$\hat{V}_{pq} = \frac{1 - \gamma(r)}{r^3} \sum_{M=-2}^{+2} C_{pq}^{2M} Y_{2M}(\Omega). \tag{6b}$$

The coefficients C_{pq}^{2M} take the values:

$$C_{xx}^{20}=C_{yy}^{20}=-2C_{zz}^{20}=-\frac{1}{2}\sqrt{\frac{16\pi}{5}},$$

$$C_{xx}^{2,2}=-C_{yy}^{2,2}=C_{xy}^{2,-2}=\frac{3}{2}\sqrt{\frac{16\pi}{15}}, \tag{7}$$

$$C_{xz}^{2,1}=C_{yz}^{2,-1}=3\sqrt{\frac{4\pi}{15}}.$$

3. Approximations

3.1. Quadrupole Polarizability

We are interested to calculate the EFG at the nucleus of ^{57}Fe in iron-containing molecular systems; therefore we need for the numerical integration of the atomic expectation values $\langle\psi_\mu|\hat{V}_{pq}|\psi_\nu\rangle$ in Eq. (5) the analytic form of $(1-\gamma(r))_{\mathrm{Fe}}$. Since we could not find an analytic formula for $\gamma(r)_{\mathrm{Fe}}$ in the literature we derived $(1-\gamma(r))_{\mathrm{Fe}}$ following approximately the lineshape [8] of $(1-\gamma(r))_{\mathrm{Cu}^+}$, and using the known shielding- and antishielding factors, R and γ_∞, for iron [1, 4]:

$$R=\frac{\langle\gamma(r)r^{-3}\rangle_{3\mathrm{d}}}{\langle r^{-3}\rangle_{3d}}=0.32, \tag{8a}$$

$$\gamma_\infty=\lim_{r\to\infty}\gamma(r)=-9.1. \tag{8b}$$

(The corresponding value for γ_∞ for Cu^+ is -9.7 [8]).

We approximate $(1-\gamma(r))$ by a set of two equations, one for small and one for large r-values:

$$1-\gamma(r)=(1-\gamma_\infty)ar^3,\ 0\leqslant r\leqslant r_0; \tag{9a}$$

$$1-\gamma(r)=(1-\gamma_\infty)\left[1-\frac{1}{(r-b)^5}\right],\quad r_0\leqslant r\leqslant\infty. \tag{9b}$$

The choice of the r^3-dependency of $1-\gamma(r)$ in Eq. (9a) guarantees that the integrand during the integration procedure of $\langle\psi_\mu|\hat{V}_{pq}|\psi_\nu\rangle$ does not become infinite for small r values. The constant a in Eq. (9a) follows from the condition that integrating the radial part of $\langle\psi_\mu|\hat{V}_{pq}|\psi_\nu\rangle$ for an iron $3d$-valence electron leads to

$$\int_0^\infty f_{3d}(r)\frac{1-\gamma(r)}{r^3}\,f_{3d}(r)r^2\,dr=(1-\gamma_\infty)a=(1-R)\langle r^{-3}\rangle_{3d}, \tag{10a}$$

or, which is equivalent

$$a=\frac{1-R}{1-\gamma_\infty}\langle r^{-3}\rangle_{3d}. \tag{10b}$$

Eq. (9b) takes care of the fact that $\gamma(r)$ is close to γ_∞ if r takes large values. The

constant b and the r-value r_0 from Eq. (9) is obtained by requiring that $(1-\gamma(r))$ can be differentiated for all r values. Thus, we get the conditions:

$$ar_0^3 = 1 - \frac{1}{(r_0 - b)^5}, \tag{11a}$$

and

$$3ar_0^2 = \frac{5}{(r_0 - b)^6}. \tag{11b}$$

In Fig. 1 we plot the $(1-\gamma(r))$ curve for ^{57}Fe, which we derive from Eqs. (9–11) and compare this result with the corresponding curve for Cu^+.

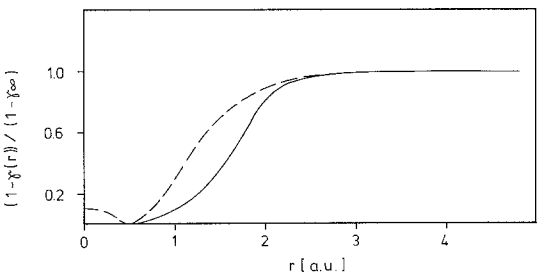

Fig. 1. Graphic presentation of $(1-\gamma(r))$ normalized to $(1-\gamma_\infty)$ as derived from Eqs. (9, 10) for iron (solid line), and for Cu^+ (dashed line, Ref. [8])

3.2. Integrals

Depending on the center to which AO's ψ_μ and ψ_ν in Eq. (5) belong, we distinguish various valence electron contributions to the EFG tensor V_{pq} at the nuclear site of atom A:

$$V_{pq}^{\text{valence electrons}} = V_{pq}^{\text{val, A–A}} + V_{pq}^{\text{val, B–B}} + V_{pq}^{\text{val, A–B}} + V_{pq}^{\text{val, B–C}}. \tag{12}$$

The various terms are discussed in the following:

1) μ and ν both belong to the (Mössbauer) atom A, then $V_{pq}^{\text{val, A–A}}$ describes the contribution of the EFG at A by the valence electrons of A:

$$V_{pq}^{\text{val, A–A}} = -e_0 \sum_{\mu\nu} P_{\mu\nu} \int_0^\infty f_\mu(r) \frac{1-\gamma(r)}{r^3} f_\nu(r) r^2 \, dr \tag{13}$$

$$\times \sum_{M=-2}^{+2} C_{pq}^{2M} \int Y_{l_\mu m_\nu}(\Omega) Y_{2M}(\Omega) Y_{l_\nu m_\nu}(\Omega) \, d\Omega.$$

The analytic integration of the radial part yields:

$$\int_0^\infty f_\mu(r) \frac{1-\gamma(r)}{r^3} f_\nu(r) r^2 \, dr = (1-R)\langle r^{-3}\rangle_{\mu\nu}. \tag{14}$$

The analytic integration over the angular part of Eq. (13) is worked out in terms of

products of Clebsch–Gordon coefficients [9]:

$$C_{pq}^{l_\mu m_\mu l_\nu m_\nu} = \sum_{M=-2}^{+2} C_{pq}^{2M} \int Y_{l_\mu m_\mu}(\Omega) Y_{2M}(\Omega) Y_{l_\nu m_\nu}(\Omega)\, d\Omega. \tag{15}$$

2) μ and ν both belong to the ligand atom B, then $V_{pq}^{\text{val, B–B}}$ is the contribution to the EFG at A by the valence electrons of B:

$$V_{pq}^{\text{val, B–B}} = -e_0(1-\gamma_\infty) \sum_{\text{B}} \sum_{\mu} P_{\mu\mu}^{\text{B}} \frac{3R_p^{\text{B}} R_q^{\text{B}} - \delta_{pq} \cdot (R^{\text{B}})^2}{(R^{\text{B}})^5}. \tag{16}$$

Eq. (16) includes the approximation that the valence electrons of ligand B are located at the atomic site of B, which is given by the space vector $\boldsymbol{R}^{\text{B}} = (R_x^{\text{B}}, R_y^{\text{B}}, R_z^{\text{B}})$ with respect to center A. Especially in the cases where the interatomic distance between A and B, R^{B}, is small compared to the radial distribution of $\sum_\mu |\psi_\mu|^2$ around B, Eq. (16) might be a too crude approximation. We therefore also calculate (see Eq. (5))

$$^*V_{pq}^{\text{val, B–B}} = -e_0 \sum_{\text{B}} \sum_{\mu\nu} P_{\mu\nu}^{\text{B}} \langle \mu | \hat{V}_{pq} | \nu \rangle \tag{17}$$

by a threedimensional numerical integration method (see appendix) for the three cases that $\psi_\mu = \psi_\nu$ is represented by Slater type $2p_z$, or $2p_x$, $2p_y$ or by $2s$ orbitals at center B. From comparison of $V_{pq}^{\text{val, B–B}}$ with the approximation of Eq. (16) we extract a multiplication factor $f^{\text{val, B–B}}$ from

$$^*V_{pq}^{\text{val, B–B}} = f^{\text{val, B–B}} V_{pq}^{\text{val, B–B}}. \tag{18}$$

In Fig. 2 we plot $f^{\text{val, B–B}}$ against R^{B}. For $R^{\text{B}} \gtrsim 0$ the correction factor $f^{\text{val, B–B}}$ approaches zero, because $V_{pq}^{\text{val, B–B}}$ from Eq. (16) approaches infinity, but $V_{pq}^{\text{val, B–B}}$ becomes zero or at least a finite number.

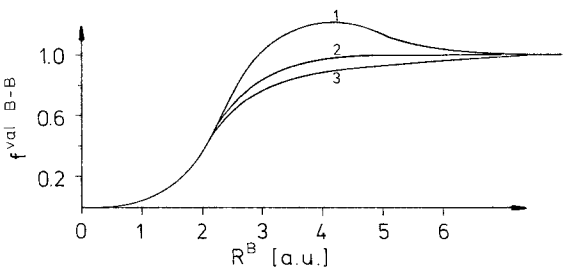

Fig. 2. Correction factor $f^{\text{val.B–B}}$ (see Eq. (18)) depending on the iron ligand distance R^{B} calculated for a ligand $2p_z^2$ electron configuration (curve 1), for a ligand $2p_x^2$, $2p_y^2$ electron configuration (curve 2), and for a ligand $2s^2$ electron configuration (curve 3)

3) μ belongs to the (Mössbauer) center A and ν to a ligand atom B, then $V_{pq}^{\text{val, A–B}}$ takes care of the contribution to the EFG at A by the bonding electrons between center A and the surrounding ligands B. The angular integration over three spherical harmonics is reduced to an integration over two spherical harmonics

[9, 10] leading to

$$V_{pq}^{\text{val, A–B}} = -e_0 \sum_{\mu\nu} 2P_{\mu\nu} \int_0^\infty f_\mu(r) \frac{1-\gamma(r)}{r^3} f_\nu(r') r^2 \, dr \tag{19}$$

$$* \sum_{L'M'} C_{pq}^{l_\mu m_\mu L'M'} \sum_{\sigma=-l_-}^{+l_-} D_{L'M'}^{\sigma} D_{l_\nu m_\nu}^{\sigma} \int Y_{L'M'}(\Omega) Y_{l_\nu m_\nu}(\Omega') \, d\Omega,$$

with $l_- = \min(L', l_\nu)$, $|l_\mu - 2| \leqslant L' \leqslant l_\mu + 2$, and $M' = 0, \pm 1, \ldots, \pm L'$.

The remaining integrals are evaluated by a twodimensional numerical integration method (see appendix) since the ζ-integration can be carried out analytically. Concerning the optimization of computing time it is important to note than in practice the integrals in Eq. (19) only depend on l_μ and l_ν of the AO's ψ_μ and ψ_ν, but not on the formal quantum numbers m_μ and m_ν.

4) μ belongs to ligand B and ν to ligand C, then $V_{pq}^{\text{val, B–B}}$ contains the contributions to the EFG at A by the overlap charges $[\psi_\mu^{\text{B}}(r, \vartheta, \varphi)\psi_\nu^{\text{C}}(r', \vartheta', \varphi')]r^2 \, dr \, d\Omega$ between ligand B and ligand C:

$$V_{pq}^{\text{val, B–C}} = -e_0 \sum_{\mu\nu} P_{\mu\nu} \sum_{\sigma=-l_-}^{+l_-} D_{l_\mu m_\mu}^{\sigma} D_{l_\nu m_\nu}^{\sigma} \int f_\mu(r) Y_{l_\mu m_\mu}(\Omega)$$

$$\times \frac{3r_p r_q - r^2 \delta_{pq}}{r^5} [1-\gamma(r)] f_\nu(r') Y_{l_\nu m_\nu}(\Omega') r^2 \, dr \, d\Omega, \tag{20}$$

with $l_- = \min(l_\mu, l_\nu)$.

The amount of approximation involved in the calculation of $V_{pq}^{\text{val, B–C}}$ by projecting the overlap charges onto the axis, which connects B and C, has been analyzed by working out the exact threedimensional integration in Eq. (20) for the special case

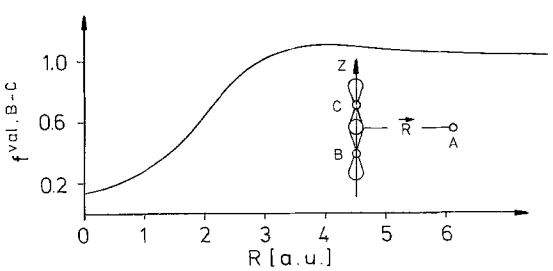

Fig. 3. Correction factor $f^{\text{val, B–C}}$ (see Eq. (21)) depending on the distance R between the center of mass of ligands B and C and the Mössbauer atom A, calculated for p_z^{B} and p_z^{C} orbitals as indicated in the insert

of p_z^{B} and p_z^{C} orbitals as indicated in Fig. 3. Comparing the approximate result V_{pq} with the "exact" value yields the correction factor

$$f^{\text{val, B–C}} = \frac{{}^*V_{pq}^{\text{val, B–C}}}{V_{pq}^{\text{val, B–C}}}, \tag{21}$$

which depends on the distance between A and the center of B–C overlap (Fig. 3).

4. Discussion

From the total electric field gradient

$$V_{pq} = V_{pq}^{\text{ligand cores}} + V_{pq}^{\text{val, A–A}} + V_{pq}^{\text{val, B–B}} + V_{pq}^{\text{val, A–B}} + V_{pq}^{\text{val, B–C}}, \tag{22}$$

which contains contributions from ligand-core charges as well as from all valence electrons, we calculate quadrupole splittings ΔE_Q and asymmetry parameters η for seven iron-containing compounds which are either characterized by ferrous low-spin ($S=0$) or ferric high-spin ($S=5/2$) state. In these cases we neglect spin-orbit coupling and calculate V_{pq} from the electronic ground state only. In agreement with this procedure the compounds under study show temperature-independent experimental quadrupole splitting. The MO calculation which yields the electronic ground state configuration Ψ for each compound has been described elsewhere [6, 11]. The atomic values α and $\Delta\alpha$ we used as MO parameters are closely related with values derived from Hartree-Fock calculations [12] and from experiments [13]. Concerning oxygen (O) we work with two different MO parameters, one for compounds containing O which is nearly neutral and one for compounds containing ionic oxygen with effective charge close to $-2e$; this procedure has been found to be reasonable in many cases [11, 14–16].

In Table 1 experimental and calculated quadrupole splittings and asymmetry parameters are listed for the seven compounds under study. The various $\Delta E_Q^{(i)}$ and $\eta^{(i)}$ values correspond to different calculational models:

1) $\Delta E_Q^{(1)}$ and $\eta^{(1)}$ are derived according to the numerical integration method described here.

2) $\Delta E_Q^{(2)}$ and $\eta^{(2)}$ result from the model that $V_{pq}^{\text{val, A–A}}$ has been calculated according to Eq. (13) and the rest of Eq. (22) has been approximated according to Eq. (2), with $q_B = q_B^{\text{eff}}$ being effective ligand charges. (The q_B^{eff} are derived from adding part of the overlap charge onto the ligand charges in order to be able to describe the dipole moment of the molecule under study by effective atomic charges only [6].)

3) $\Delta E_Q^{(3)}$ results from the model that $V_{pq}^{\text{val, A–A}}$ has been calculated according to Eq. (13) with $P_{\mu\nu}^{\text{eff}}$ instead of $P_{\mu\nu}$, and the rest of Eq. (22) has been approximated as described under 2). The effective bond order values $P_{\mu\nu}^{\text{eff}}$ result from the same procedure which led us under 2) to q_B^{eff} Model 2) which uses $P_{\mu\nu}$ and q_B^{eff}, is inconsistent with respect to model 3), which uses $P_{\mu\nu}^{\text{eff}}$ and q_B^{eff}, because part of the overlap charge has been neglected in 2).

4) $\Delta E_Q^{(4)}$ results from applying model 2) and additionally taking care of overlap contribution to V_{pq} by applying a procedure which transforms the overlap part $\langle\psi_\mu^A|\hat{V}_{pq}|\psi_\nu^B\rangle$ into the subspace of $\psi_{\mu'}^A$ leading to [17]:

$$\langle\psi_\mu^A|\hat{V}_{pq}|\psi_\nu^B\rangle = \sum_{\mu'} \langle\psi_\mu^A|\hat{V}_{pq}|\psi_{\mu'}^A\rangle\langle\psi_{\mu'}^A \mid \psi_\nu^B\rangle. \tag{23}$$

This model overestimates the overlap contribution to V_{pq} since q_B^{eff} and $\langle\psi_{\mu'}^A \mid \psi_\nu^B\rangle$ both contain overlap charge. An additional approximation involved in this model is due to the fact that in practice the AO's $\psi_{\mu'}^A$ are a limited basis set only.

Table 1. Experimental and calculated quadrupole splittings ΔE_Q^a in mms^{-1} and asymmetry parameters η for ferrous low-spin ($S=0$) and ferric high-spin ($S=5/2$) compounds

Compound	Spin state	ΔE_Q^{exp}	Ref.	$\Delta E_Q^{(1)}$	$\eta^{(1)}$	$\Delta E_Q^{(2)}$	$\eta^{(2)}$	$\Delta E_Q^{(3)}$	$\Delta E_Q^{(4)}$	$\Delta E_Q^{(5)}$	$^{(b)}M$
$Fe(C_5H_5)_2$	0	2.33 – 2.42	c–i	2.63 ± 0.24	0.0	2.89 ± 0.26	0.0	4.03	9.70	2.40	59
$Fe(C_5H_4)_2(CH_2)_3$	0	2.27 ± 0.03	g	2.63	0.23	2.73	0.16	3.90	9.73	2.28	75
$Fe(C_5H_4)_2(CH_2)_2CO$	0	2.22 ± 0.01	d	2.73	0.13	2.83	0.08	3.95	9.44	2.24	77
$[Fe(CN)_5H_2O]^{3-}$	0	0.80	j	0.92	0.05	0.82	0.05	0.87	0.86		55
$[Fe(CN)_5NH_3]^{3-}$	0	0.671 ± 0.006	k	0.69	0.14	0.76	0.13	0.77	0.94		56
$GdFeO_3$	5/2	0.02 ± 0.03	l	0.11	0.52	0.10	0.54	same as			33
Fe_2TiO_5	5/2	0.70	m	0.78	0.25	0.65	0.10	$\Delta E_Q^{(2)}$			33

[a] Calculated quadrupole splittings $\Delta E_Q^{(i)}$ are derived from $\Delta E_Q = \frac{1}{2}e^2 Q V_{ZZ}(1+\eta^2/3)^{1/2}$ with V_{ZZ} and $\eta = (|V_{xx} - V_{yy}|)/|V_{zz}|$ resulting from diagonalizing the calculated EFG tensor V_{pq} and with $Q = 0.21$ barn.

[b] M is the number of AO basis orbitals used in our MO calculations.

[c] Stukan, R. A., Gabin, S. P., Nesmeganow, A. N., Gol'danskii, U. I., Makarov, E. F.: Teor. Eksperim. Khim. **2**, 805 (1966).

[d] Good, M. L., Buttone, J., Foyt, D.: Ann. N.Y. Acad. Sci. **239**, 193 (1974).

[e] Korecz, L., Abou, H., Ortaggi, G., Graziani, M., Belluco, U., Burger, K.: Inorg. Chim. Acta **9**, 209 (1974).

[f] Epstein, L. M.: J. Chem. Phys. **36**, 2731 (1962).

[g] Nagy, A. G., Dezsi, I., Hillman, M.: submitted to J. Org. Chem. (1976).

[h] Collins, R. L.: J. Chem. Phys. **42**, 1072 (1965).

[i] Zahn, U., Kienle, P., Eicher, H.: Z. Phys. **166**, 220 (1962).

[j] Gütlich, P., in: Topics in applied physics, Gonser, U. ed., Vol. 5, p. 53. Berlin: Springer Verlag 1975.

[k] Kerler, W., Neuwirth, W., Fluck, E., Kuhn, P., Zimmermann, B.: Physik **173**, 321 (1963).

[l] Eibschütz, M., Shtrikman, S., Treves, D.: Phys. Rev. **156**, 562 (1967).

[m] Shirane, G., Cox, D. E., Ruby, S. C.: Phys. Rev. **125**, 1158 (1962).

5) $\Delta E_Q^{(5)}$ results from the model that $V_{pq}^{\text{val, A–A}}$ has been calculated according to Eq. (13) and the rest of Eq. (22) has been approximated by [3]:

$$V_{pq}^{\text{overlap+ligand}} = (1-\gamma_\infty) \sum_{\text{ab}} \frac{3R_p^{\text{ab}} R_q^{\text{ab}} - (R^{\text{ab}})^2 \delta_{pq}}{(R^{\text{ab}})^5} q_{\text{ab}}. \tag{24}$$

The summation is over all atoms a and b of the molecular system under study. In case that a=A and b=B, q_{ab} represents the overlap charge between the Mössbauer atom A and ligand B, if a=B and b=C, q_{ab} represents the overlap charge between ligands B and C, if a=b=B, q_{ab} represents the charge of ligand B. The charges q_{ab} are calculated from bond order matrix elements $P_{\mu\nu}$ and from overlap integrals $S_{\mu\nu}$:

$$q_{\text{ab}} = e_0 (Z_{\text{a}} \delta_{\text{ab}} - \sum_{\mu\nu} P_{\mu\nu} S_{\mu\nu}). \tag{25}$$

(e_0 is the positive elementary charge). The summation over μ includes AO's ψ_μ on center a and that of ν includes AO's ψ_ν, centered on atom b. $e_0 Z_{\text{a}}$ represents the core charge of atom a. The Cartesian coordinates R_p^{ab} and the distance R^{ab} in Eq. (24) between iron and the various overlap charges q_{ab} are chosen as if q_{ab} were situated at the maximum of product $\psi_\mu \psi_\vartheta$. Since the so defined q_{ab} have a distance R^{ab} to the Mössbauer atom larger than about 1.5 Å the use of $(1-\gamma_\infty)=10.1$ is adequate in most cases [8].

Comparing experimental and theoretical results in Table 1 we find that the various calculational models for V_{pq} lead to nearly equal results if the compound under study is highly ionic ($GdFeO_3$ and Fe_2TiO_5) or if the point symmetry of the Mössbauer atom is relatively high (the latter condition implies that several V_{pq} contributions cancel each other). The more covalency, i.e. the more overlap charge is involved, and the more deviation from octahedral or tetrahedral point symmetry of the Mössbauer atom is included, the more critical the influence of approximations applied to estimate the overall EFG-tensor V_{pq} may become. This

Table 2. Various contributions to the electric field gradient component V_{ZZ} (in mms^{-1}) according to model 1) for $Fe(C_5H_5)_2$ and $[Fe(CN)_5NH_3]^{3-}$, calculated with 100 abscissas

Electric field gradient contributions		$Fe(C_5H_5)_2$	$[Fe(CN)_5NH_3]^{3-}$
$V_{ZZ}^{\text{val, A–A}}$	From Fe 3*d*	+ 4.295	+0.348
	From Fe 4*p*	− 1.267	+0.107
$V_{ZZ}^{\text{val, B–B}}$		−12.379	−7.546
$V_{ZZ}^{\text{val, A–B}}$	From Fe 3*d*-B	− 0.405	+0.201
	From Fe 4*s*-B	+ 0.344	−0.047
	From Fe 4*p*-B	+ 2.432	−0.223
$V_{ZZ}^{\text{val, B–C}}$	From next nearest neighbors	− 5.765	+0.147
	From next neighbors	+ 0.753	
$V_{ZZ}^{\text{ligand cores}}$		14.679	7.700
For comparison:			
$V_{ZZ}^{\text{val.B–B}}$ as derived from $q_{\text{B}}^{\text{eff}}$; see model 2)		− 0.135	+0.301

is shown drastically by the various $\Delta E_Q^{(i)}$ values of the three sandwich compounds $Fe(C_5H_2)_2$, $Fe(C_5H_4)_2(CH_2)_3$ and $Fe(C_5H_4)_2(CH_2)CO$.

In order to show the various contributions (which result from model 1)) to V_{pq} individually we tabulate for $Fe(C_5H_5)_2$ and $[Fe(CN)_5NH_3]^{3-}$ the V_{ZZ} components in Table 2. The considerable amount of overlap contribution $V_{ZZ}^{val,A-B}$ in ferrocene is due to the relatively large amount of overlap charge, and also due to the specific geometric arrangement of ligands in this molecule, which implies that all V_{ZZ} contributions in Eq. (22) besides $V^{val,A-A}$ are enhanced by a factor of 10, because we are concerned with 10 identical ligands (CH-groups) B, each contributing equally to V_{ZZ}. Additionally, it is important to note that Fe 4*p* electrons contribute considerably to V_{pq}, and even Fe 4*s* contributions in $V_{pq}^{val,A-B}$ are significant.

The error in $\Delta E_Q^{(1)}$, $\Delta E_Q^{(2)}$ and $\Delta E_Q^{(5)}$ of ferrocene, as indicated in Table 1, is due to uncertainties in the X-ray structure analysis; changes of the inter-ring distance in $Fe(C_5H_5)_2$ by ± 0.02 Å yield $\delta(\Delta E_Q^{(1)}) = \pm 0.24$ mms^{-1}.

The $\Delta E_Q^{(i)}$ values in Table 1 have been calculated with the use of nuclear quadrupole moment $Q = 0.21$ barn [17]. An alternative value is derived from Fig. 4, where we compare ΔE_Q^{exp} with V_{pq}^{calc}, which is given in terms of $1/2\ e^2\ V_{zz}(1+\eta^2/3)^{1/2}$. The slope of the solid line, which results from a least square fit of experimental data, corresponds to $Q = 0.18 \pm 0.03$ barn; this value has been used in the literature already before [18, 19]. For comparison the dashed line with $Q = 0.21$ barn is also given in Fig. 4.

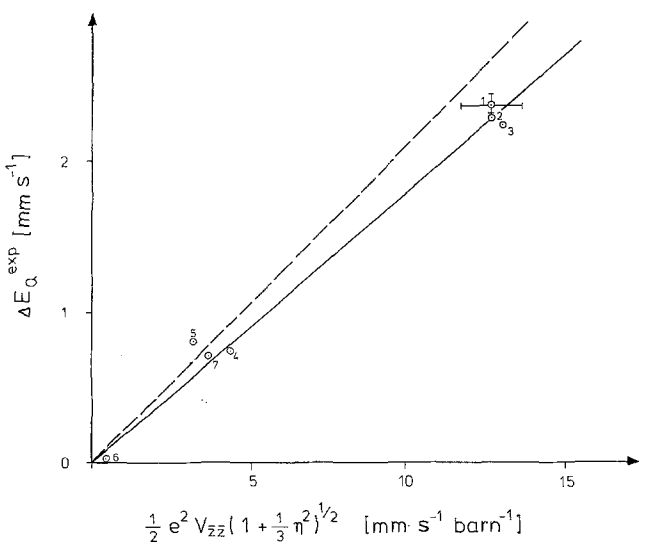

Fig. 4. Experimental quadrupole splittings ΔE_Q at 300°K and calculated electric field gradients in terms of $\frac{1}{2}e^2V_{ZZ}(1+\eta^2/3)^{1/2}$ for the compounds listed in Table 1. The solid line is a least square fit to the experimental points with a slope of $Q = 0.18$ barn (nuclear quadrupole moment); for comparison the dashed line which corresponds to $Q = +0.21$ barn, (1 mms^{-1} barn$^{-1} = 4.78 \cdot 10^{16}$ eV cm^{-2})

Since the numerical integration method is relatively time-consuming it is worthwhile to check whether in cases with large AO basis sets the amount of additional information obtained by this method balances the expense of computer time. A molecular system with $M=50$ basis orbitals (we use 59 for ferrocene) requires about 6400 basis integrals to calculate $\Delta E_Q^{(1)}$, where each integral takes about $t(V_{pq})=38$ ms of computer time.[1] $t(V_{pq})$ increases with M^2, and with the number of abscissas above 100 does not increase the accuracy of the final results of V_{pq} (or of ΔE_Q) but considerably increases the computer time $t(V_{pq})$ to calculate V_{pq} (Table 3).

Table 3. Influence of the amount of abscissas n within the numerical integration method upon the total computer time $t(V_{pq})$ to evaluate the electric field gradient tensor V_{pq}, and upon the accuracy of the calculated quadrupole splitting ΔE_Q in ferrocene ($Fe(C_5H_5)_2$)

n	$t(V_{pq})$ in s	ΔE_0 in mms^{-1}
36	252	3.07
100	374	2.68
256	641	2.62
484	1024	2.63

Appendix

The numerical integration method is based on a Gaussian type integration rule [20, 21]. Each integral is represented by:

$$\int_{-1}^{+1} f(x)\,dx = \sum_{i=1}^{n} a_i f(x_i). \tag{A1}$$

The numerical integration of EFG tensor matrix elements is based on two-dimensional integrals, having the form:

$$\int_0^{\infty} dx \int_{-1}^{+1} dy f(x, y).$$

Substituting $x=\ln 2-\ln(1+z)$ the above integral transforms so that the above integration rule (Eq. (A1)) is applicable:

$$\int_0^{\infty} dx \int_{-1}^{+1} dy f(x, y) = \int_{-1}^{+1} \frac{dz}{1+z} \int_{-1}^{+1} dy f[x(z), y]. \tag{A2}$$

It turns out that the twodimensional integrals under study here are derived with about 3% accuracy using $n^2=100$ abscissas.

A further test of the accuracy of the numerical integration method was performed by calculating overlap integrals which usually are derived by analytic integration [6, 10]. For a representative $2p_z$-$2p_z$-overlap integral the exact value is -0.07313

[1] The computer work was carried out at the TR 440 of the "Rechenzentrum der Universität des Saarlandes".

while the numerical result yields -0.07121 based on 100 abscissas or -0.07255 based on 400 abscissas.

References

1. Ingalls, R.: Phys. Rev. **128**, 1155 (1962)
2. Trautwein, A., Harris, F. E., Dezsi, I.: Theoret. Chim. Acta (Berl.) **35**, 231 (1974)
3. Trautwein, A., Reschke, R., Dezsi, I., Harris, F. E.: J. de Phys. **37**, C6, 463 (1976)
4. Sternheimer, R. M.: Phys. Rev. **80**, 102 (1950); Phys. Rev. **84**, 244 (1951); Phys. Rev. **95**, 736 (1954); Phys. Rev. **105**, 158 (1957)
5. Pople, J. A., Beveridge, D. L.: Approximate molecular orbital theory. New York: McGraw-Hill 1970
6. Rein, R., Clarke, G. A., Harris, F. E.: Quantum aspects of heterocyclic compounds in chemistry and biochemistry II. Israel Academy of Sciences and Humanities 1970
7. Löwdin, P. O.: Phys. Rev. **97**, 1474 (1955)
8. Foley, H. M., Sternheimer, R. M., Tycko, D.: Phys. Rev. **93**, 734 (1954)
9. Edmonds, A. R.: Drehimpulse in der Quantenmechanik. Mannheim, Wien, Zürich: Bibliographisches Institut
10. Harris, F. E.: Computational methods of quantum chemistry. TXVII prepared for the 1967 Summer Institute in Quantum Chemistry, Solid State Physics and Quantum Biology, Uppsala, Sweden
11. Trautwein, A., Harris, F. E.: Theoret. Chim. Acta (Berl.) **30**, 45 (1973)
12. Fraga, S., Karwowski, J.: Tables of Hartree-Fock atomic data. University of Alberta, Edmonton, Canada T6G2G2
13. Moore, C. E.: Atomic energy levels. Cur. Nat. Bur. Std. (1949)
14. Zimmermann, R., Trautwein, A., Harris, F. E.: Phys. Rev. **B12**, 3902 (1975)
15. Trautwein, A., Kreber, E., Gonser, U., Harris, F. E.: J. Phys. Chem. Solids **36**, 325 (1975)
16. Reschke, R., Trautwein, A., Desclaux, J. P.: J. Phys. Chem. Solids **38**, 837 (1977)
17. Trautwein, A., Reschke, R., Zimmermann, R., Dézsi, I., Harris, F. E.: J. de Phys. **35**, C6, 235 (1974)
18. Ingalls, R. I.: Phys. Rev. **133**, A787 (1964)
19. Johnson, C. E.: Proc. Phys. Soc. (London) **92**, 748 (1967)
20. Zurmühl, R.: Praktische Mathematik. Berlin, Heidelberg, New York: Springer Verlag 1965
21. Davis, Ph. J., Rabinowitz, Ph.: Methods of numerical integration. New York: Academic Press 1975

Received June 2, 1977/August 31, 1977